Chapter 4

Analytical imaging studies clarifying the process of the darkening of vermilion in paintings

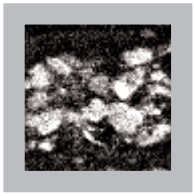

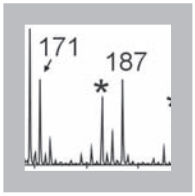

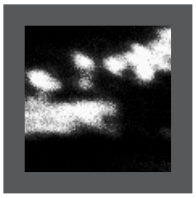

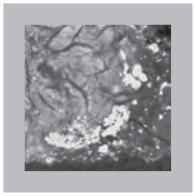

Imaging-secondary ion mass spectrometry (SIMS) is applied for the first time to paint cross-sections with degraded vermilion (red mercury sulphide) paint to cast new light on the well-known problem of its light induced darkening. The static SIMS data are combined with light microscopic, electron microscopic studies and energy dispersive X-ray analysis (SEM/EDX) to identify and localise the various reaction products. The spatial distribution of atomic and molecular species in paint cross-sections of the native vermilion and the reaction products leads to the formulation of a new hypothesis on the reaction mechanism of the photo-degradation of vermilion where two black and white coloured reaction products are formed sequentially. Under the influence of light some of the vermilion (HgS) is converted into Hg(0) and S(0). In this process the chlorine ions, present in the native vermilion, act as a catalyst. We propose that the Hg(0) is deposited on the surface of the remaining HgS as elementary mercury nanoparticles, which turns the vermilion black. Chloride, derived from an external source, is accumulating in the black phase. The metallic mercury and the remaining HgS react away with the excess of chloride. Two intermediate products and a white end product, mercuric chloride ($HgCl_2$), are formed.

4.1 Introduction

Blackening of vermilion (HgS, trigonal), a light induced degradation phenomenon of HgS, is observed on the raw mineral cinnabar as well as on vermilion paint in works of art. The colour change may strongly disfigure the painted image.[1] The highlights in a detail of *Triumphal Procession with Sacrificial Bull* by P. de Grebber (1650) (Oranjezaal, Huis Ten Bosch Palace, The Hague, The Netherlands) should have been vivid red, but are transformed into greyish strokes (Fig. 4.1).This irreversible surface degradation process takes place irrespective of the origin of the vermilion and the type of binding medium.[1] It does not matter whether vermilion has been processed wet or dry, or is derived from a natural source as cinnabar[1]. Until recently, the black product on vermilion was thought to be meta-cinnabar (HgS, cubic).[2, 3, 4, 5] However, Dreyer suggested already in 1938 that the blackening resulted from a superficial layer of colloidal mercury in solid solution on the cinnabar and that the blacking process was accelerated by impurities.[6] McCormack and others have shown recently that halogen impurities in and around vermilion particles play a dominant role in the darkening process.[4, 7, 8] Small concentrations of chlorine in cinnabar (average between 0.05 - 1 wt%) can already cause blackening, where as cinnabar with a chlorine concentration less than 0.01 wt% remains unaffected by sunlight.[7] Not only chlorine, but also other halogens (mainly iodine), trigger the blackening of vermilion.[4, 5, 7] Recently, Spring *et al.* observed two degradation products in blackened vermilion[9], a black and white one, which were assumed to be formed simultaneously. It was inferred that vermilion is first transformed into the photo-

Fig. 4.1 Detail of 'Triumphal Procession with Sacrificial Bull' by P. de Grebber (1650) (Oranjezaal, Huis Ten Bosch Palace, The Hague, The Netherlands) showing grayish strokes on top of the red dress. These highlights consist of blackened vermilion. Photo: L. Speleers, Stichting Restauratie Atelier Limburg (SRAL), Maastricht, The Netherlands (see coloured version at the end of this thesis).

sensitive mineral corderoite ($Hg_3S_2Cl_2$) after exposure to humidity and chloride ions. This corderoite subsequently degrades into the black meta-cinnabar, the white calomel $(HgCl)_2$ and elemental sulphur by a light induced reaction. The chloride was postulated to originate from external sources.

In general, the degraded vermilion layers in paint cross-sections are extremely thin (less than a few microns) and most analytical techniques do not have sufficient spatial resolution and sensitivity to study the changes within the paint layer.[4, 9] The availability of a paint cross-section taken from a (17th century ?) overpaint on the painting *Portrait of a Young Woman* by Peter Paul Rubens (1620s) (Mauritshuis, The Hague; sample number MH251/26) with an extraordinary thick layer of partially degraded, blackened vermilion particles made it possible to investigate the degradation process in more detail (Fig. 4.2a and 4.3a). In this paper a second paint cross-section from an original layer in *Minerva and Hercules opening the doors for Victory* by Christiaan van Couwenberg (1651), (Oranjezaal Huis ten Bosch Palace, The Hague; sample number HSTB 34/2), derived from a different collection than the first sample, is examined as well.

Portrait of a Young Woman by Peter Paul Rubens (1620s) displayed in Royal Picture Gallery Mauritshuis, The Hague (inv. no. 251) (see coloured version at the end of this thesis).

An important advantage of investigating the blackening process of vermilion in paint cross-sections is the clear visualisation of a gradient in the deterioration from the light exposed top to the light shielded bottom. In addition, the pigment particles are embedded in an organic binding medium layer, so the components possibly released during the blackening of vermilion are embedded and fixed in position so they can be investigated by microscopy.

The analytical data obtained from light microscopy (LM), scanning electron microscopy combined with energy dispersive X-ray analysis (SEM/EDX) and secondary ion mass spectrometry (SIMS) presented here lead to new insight in the mechanism of the blackening of vermilion. In contrast to work presented earlier,[9] we observe that a black reaction product is formed first, which is spatially separated and thus followed by a white compound. We prove that meta-cinnabar cannot be formed and with the exclusive results from secondary ion mass spectrometry, we could identify another white reaction product that was never before described in paintings.

4.2 Experimental

4.2.1 Samples

The paint sample MH251/26 was embedded in polyester resin Polypol using the Easysection™ system. Sample HSTB 34/2 was embedded in Technovit® 2000LC (Heraeus Kulzer, Germany). Both paint cross-sections were dry polished with Micromesh® polishing cloths (final step 12 000 mesh) (Scientific Instruments Services Inc., Minnesota). The following reference materials were used: mercury sulphide (HgS) (Merck), mercuric chloride ($HgCl_2$) (Merck) and mercurous chloride ($(HgCl)_2$) (Fluka).

4.2.2 Instruments

The static SIMS experiments were performed on a Physical Electronics (Eden Prairie, MN) TRIFT-II time-of-flight SIMS (TOF-SIMS). The surface of the sample was scanned with a 15 KeV primary ion beam from an $^{115}In^+$ liquid metal ion gun. The pulsed beam was non-bunched with a pulse width of 20 ns, a current of 600 pA and a spot size approximately 120 nm. The primary beam was rastered over a 50 x 50 µm sample area, divided into 256 x 256 pixels. The surface of the sample was charge compensated with electrons pulsed in between the primary ion beam pulses. To prevent large variations in the extraction field over the large insulation surface area of the paint cross-section a non-magnetic stainless steel plate with slits (1 mm) was placed on top of the sample. The paint cross-section (150 x 50 x 3 mm) was rinsed in hexane to eliminate contamination of airborne silicones.

A 15 KeV $^{115}In^{+}$ primary ion beam was used for the reference samples, with primary ion pulses that were compressed (bunched) to ~1 ns to obtain a better mass resolution. These experiments were performed with 600 pA beam current. All these measurements were charge compensated with electrons pulsed in between the primary ion beam pulses. The oil immersion reflected light microscopic images were obtained on a Leica DMRX microscope (Leica, Wetzlar, Germany). White light was provided by a 100 W halogen lamp, and an Osram HBO 50 W lamp and Leica filter D (excitation 360-425 nm, emission > 460 nm) were used for fluorescence microscopy. The surface of the paint cross-section was covered with immersion oil (cat. nr. 11 513 787, Leica, Germany) Images were recorded with a Nikon digital still camera DXM1200 (Nikon Instech Co., Ltd., Japan).

Scanning Electron Microscopy studies in combination with Energy Dispersive X-ray analysis (SEM-EDX) were performed on a XL30 SFEG high vacuum electron microscope (FEI, Eindhoven, The Netherlands) with EDX system (spot analysis and elemental mapping facilities) from EDAX (Tilburg, The Netherlands). Backscattered electron images of the cross-sections were taken at 20 kV accelerating voltage at a 5 mm eucentric working distance and a spot size of 3, which corresponds to a beam diameter of 2.2 nm with current density of approximately 130 pA. EDX analysis was performed at a spot size setting of 4 (beam diameter 2.5 nm and current density 550 pA) to obtain a higher count rate and at an acceleration voltage of 20 kV. EDX Mapping parameters were: 256 x 200 matrix, 1028 frames, 100 µs dwell time and 50 µs amplitude time. Samples were carbon coated to improve surface conduction in a CC7650 Polaron Carbon Coater with carbon fibre (Quorum Technologies, East Sussex, UK).

4.3 Results

4.3.1 Light microscopy

Light microscopic images of a highly magnified area of discoloured vermilion in the paint cross-section MH251/26 are shown in Fig. 4.2a, 4.3a and 4.4a (normal light) and 4.2b and 4.3b (UV light). The area of the panel painting of the sample MH251/26 is overpainted and the paint build up consist now of at least six layers. The original paint layers consist of a chalk ground, a lead white- and charcoal-containing imprimatura and finally several layers of vermilion and red lake. A bone black layer blocks out this original red paint. On top a thin organic intermediate layer is applied with as final layer the now degraded vermilion with red lake (paint cross-section not shown). The total thickness of the vermilion layer is 25 mm of which 15 mm is discoloured, containing both the black and white degradation products. The vermilion particles are coarse grained

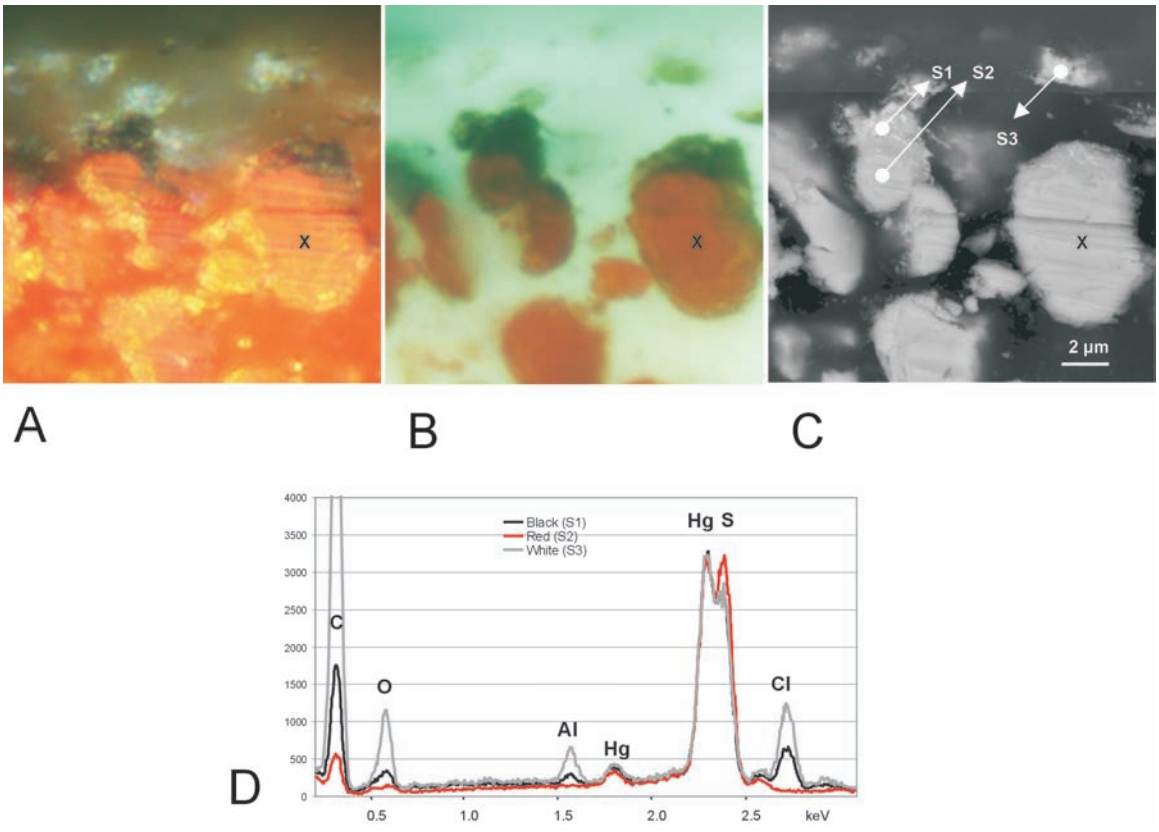

Fig. 4.2 Light microscopic image under white light (A) and UV illumination (B) illustrating the partial photodegradation of a vermilion particle. The backscattered electron image (BSE) (C) shows the structural difference between the red and the black area. The horizontal lines are due to polishing, the text refers to the particle marked X. EDX spectra of spot analyses (D) in black (S1), red (S2) and white (S3) area demonstrate the different elementary compositions of the native material and the reaction products (see coloured version at the end of this thesis).

and the individual particles are partially degraded in some instances. These latter particles consist of a black upper part and a red lower part (in UV light the colours remain black and red). The white product is positioned on top and around the black product and is transparent under UV illumination.

A magnified area of the darkened vermilion in paint cross-section HSTB 34/2 is shown in Fig. 4.5a and b (normal and UV light). There are three layers in the area of the panel painting where the sample was removed: a grayish lead white ground, a reddish-brown iron oxide paint layer and on top a red paint layer with a mixture of vermilion and red lake (paint cross-section not shown). The degraded top layer with black and white products is very thin (4 mm), while the total thickness of the vermilion and red lake layer is 50 mm. The intact layer consists mainly of finely dispersed vermilion particles with a few larger ones. The red lake in the vermilion layer is recognisable by the pinkish fluoresce in the UV image (Fig. 4.5b).

4.3.2 SEM/EDX

The backscattered electron image (BSE-image) illustrates the presence of a structural change in the partially degraded vermilion particle of MH251/26 (Fig. 4.2c). The structure of the red vermilion particle differs from the structure of the black product. The red part of particle X (indicated in Fig. 4.2c) is flat and homogeneous. The horizontal lines in the particles are polishing marks. The black part of the particle X is irregular and broken up. Spots with a higher BSE intensity and a size smaller than 100 nm are visible in the degraded black phase (Fig. 4.2c and supplementary Fig. 4.1). The white areas display the same BSE intensity as the black and the red areas.

The two elements in vermilion - mercury and sulphur - are detected with EDX spot analysis in the red (S2), black (S1) and white (S3) particles (Fig. 4.2d). EDX spot analyses of the red (S2), black (S1) and the white (S3) phases demonstrate that there is relatively less sulphur in the degraded particles (Fig. 4.2d), considering the sulphur/mercury ratio. This sulphur/mercury ratio is only indicative because the X-ray intensity peaks of the mercury *M*-shell and the sulphur *K*-shell are partially overlapping. EDX spot analysis from the black area (S1) and white area (S3) show relatively high chlorine counts; the chlorine concentration in the white particle is much higher than in the black particle (taking the mercury peak as reference). The EDX spectrum of the white area reveals that the intensities of carbon, oxygen and aluminium are high compared to the black and red area. However, these elements are representative for the organic binding medium and are only detected due to the fact that the interaction volume of the beam is larger than the volume of the particle. The sulphur to mercury ratio in the binding medium of both the degraded and intact part is higher than the red particles (spectrum not shown), which indicates that sulphur besides being a constituent of HgS, is also present in another

form in the binding medium.
Elemental X-ray maps of the affected vermilion layer in MH251/26 visualise the distribution of mercury, sulphur and chlorine (Fig. 4.3). The dotted line in the elemental images indicates the compositional transition between red (R) and black (B) particles (Fig. 4.3). The elemental X-ray map of mercury illustrates that mercury is only present inside the pigment particles and has not diffused into the binding medium. Sulphur is present in high relative intensity in the mercury-containing particles of the intact layer (R), whereas lower sulphur X-ray counts are observed in and around the degraded particles (B). The chlorine is only detected in high counts in the degraded vermilion particles.

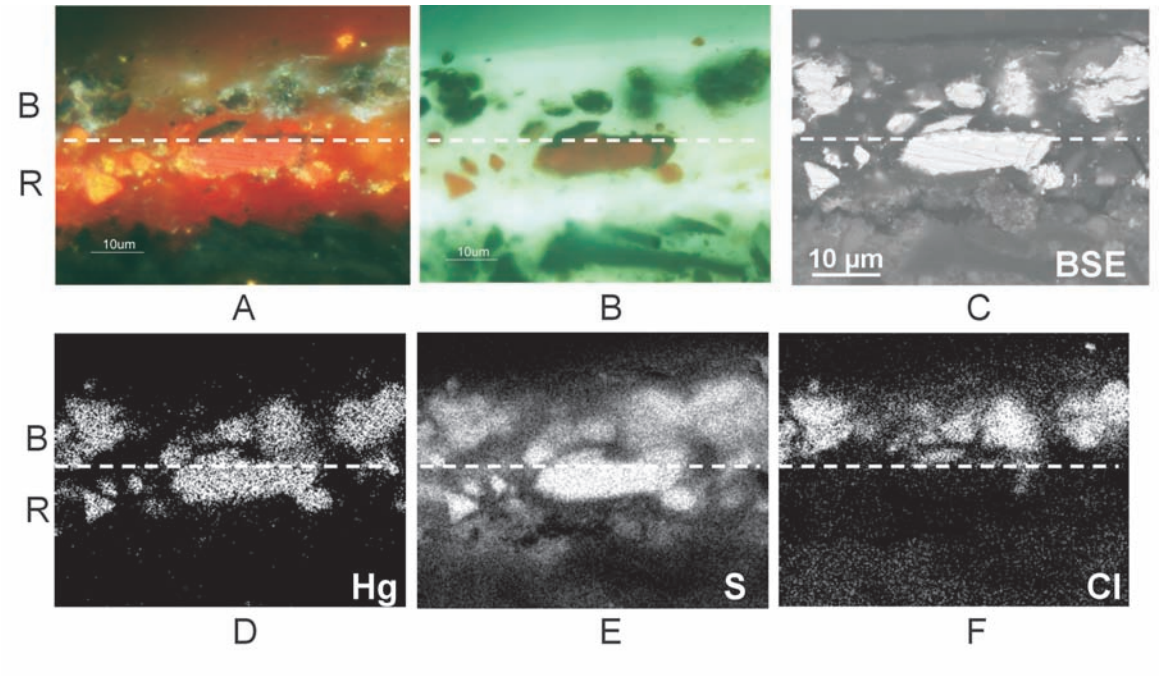

Fig. 4.3 The light microscopic images under white light (A) and UV light (B) illumination and back-scattered electron image (BSE)(C) of the partially degraded vermilion paint in paint cross-section MH251/26 corresponding with the area analysed by EDX imaging. X-ray maps of intact (R) and blackened (B) vermilion in the layer reveals the spatial distribution of mercury (Hg L)(D), sulphur (S K)(E) and chlorine (Cl K)(F) (see coloured version at the end of this thesis).

4.3.3 SIMS

SIMS spectra were acquired in the negative ion mode. Chloride and sulphide dominate in the SIMS spectra of MH251/26 and HSTB 34/2. The spatial distribution of the sulphide and chloride ions in sample MH251/26 is plotted in Fig. 4.4b and 4.4c, respectively. Fig. 4.4a represents the light microscopic image of the scanned SIMS area. Three horizontal lines in the images in Fig. 4.4 outline the blackened layer (B) and the red vermilion layer (R). The intact red vermilion particles contain sulphide and chloride (see layer R in Fig. 4.4b and c). The chloride is present in higher amounts in the degraded

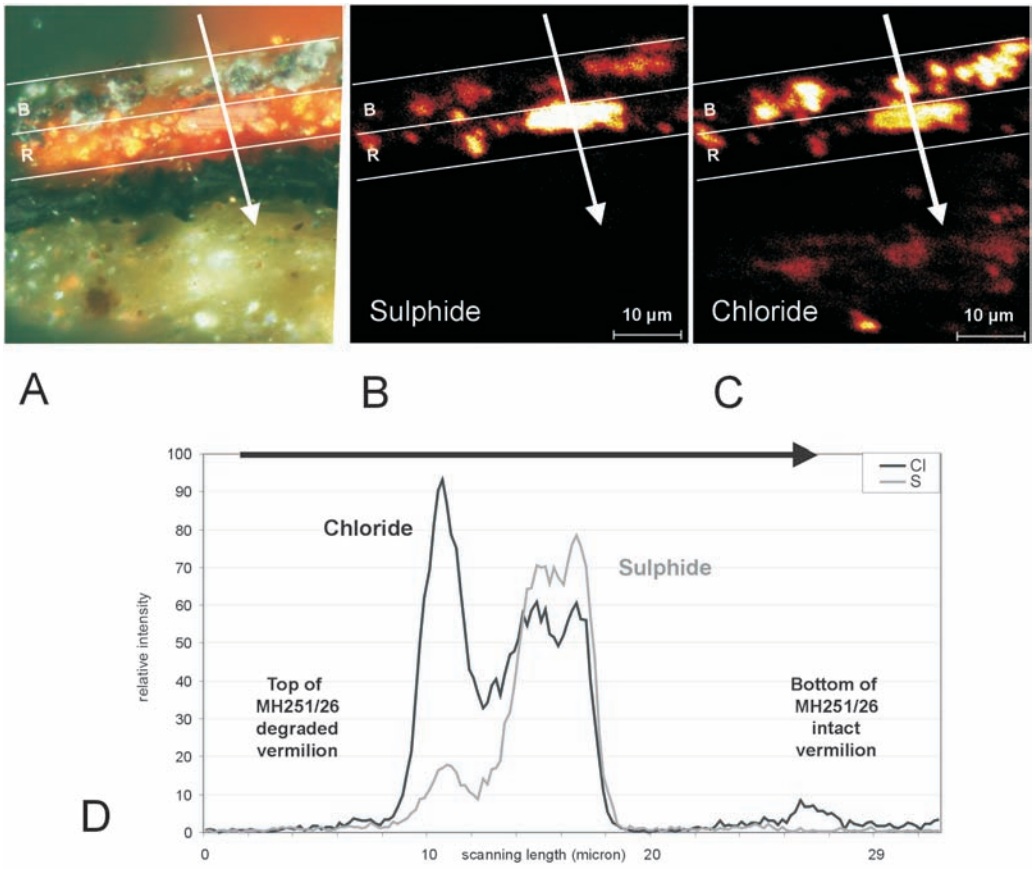

Fig. 4.4 The arrow in the light microscopic image (A), which is representing the scanned SIMS area of the partially degraded vermilion paint in MH251/26, indicates the direction of the line scan. SIMS images of the sulphide (B) and chloride (C) represent the distribution of these ions over the partially degraded vermilion paint layer. The line scan (D), illustrates the distribution of chlorine and sulphur from top to bottom in the paint cross-section (see coloured version at the end of this thesis).

layer (B) and corresponds to the black and white particles. Line scans drawn from the top to the bottom of the layer (see white arrows in Fig. 4a, b and c) visualise the distribution of the secondary ion yields. The secondary ion yields of both chloride and sulphide ions are depicted in Fig. 4.4d. The line scan, with a resolution of 1 mm, first crosses a degraded vermilion particle (3 mm) and then scans an intact vermilion particle (5 mm). The chloride ion yield is higher for degraded vermilion compared to the intact vermilion. The sulphide ion yield is relatively diminished in the degraded particles compared to the intact vermilion. The same phenomenon is observed in paint cross-section HSTB 34/2 (Fig. 4.5c). The line scan crosses the degraded vermilion layer (4 mm) and two intact vermilion particles (6 mm) (Fig. 4.5a, b and c). The chloride and sulphide ion distribution are displayed in Fig. 4.5d and e.

Similar negatively charged mercury-halogen cluster ion patterns were detected in the paint cross-sections MH251/26 and HSTB34/2. The corresponding molecules were deduced on the basis of their molecular weight distribution and isotopic pattern. The

SIMS spectra of HSTB 34/2 show the cluster ions from $[Hg_nS_nCl]^-$ (n = 1-6), $[Hg_nS_{n-1}Cl_3]^-$ (n = 1-4) and $[Hg_nS_{n+1}Cl_2]^-$ (n = 1-3). The spectra of sample MH251/26 show the same types of cluster ions, but only for n = 1-2 (full spectra not shown, a partial negative ion spectrum of HSTB 34/2 with n = 3 is discussed in the next paragraph). The ions are interpreted as chloride adduct ions from $(HgS)_n$ [$(HgS)_n \cdot Cl^-$ (n = 1-6)], $(HgS)_n(HgCl_2)$ [$(HgS)_n(HgCl_2) \cdot Cl^-$ (n = 0-3)] and $(HgS)_n(SCl)$ [$(HgS)_n(SCl) \cdot Cl^-$ (n = 1-3)], respectively. Other types of cluster ions detected with lower ion yields in the paint sample are $(HgCl)_2 \cdot Cl^-$ and $Hg_nS_yCl^-$ ($y = n + 1$, $n + 2$ or $n + 3$). $(HgS)_n \cdot Cl^-$, $(HgS)_n(SCl) \cdot Cl^-$ and $Hg_nS_yCl^-$ are detected in the intact and degraded vermilion particles of HSTB 34/2,

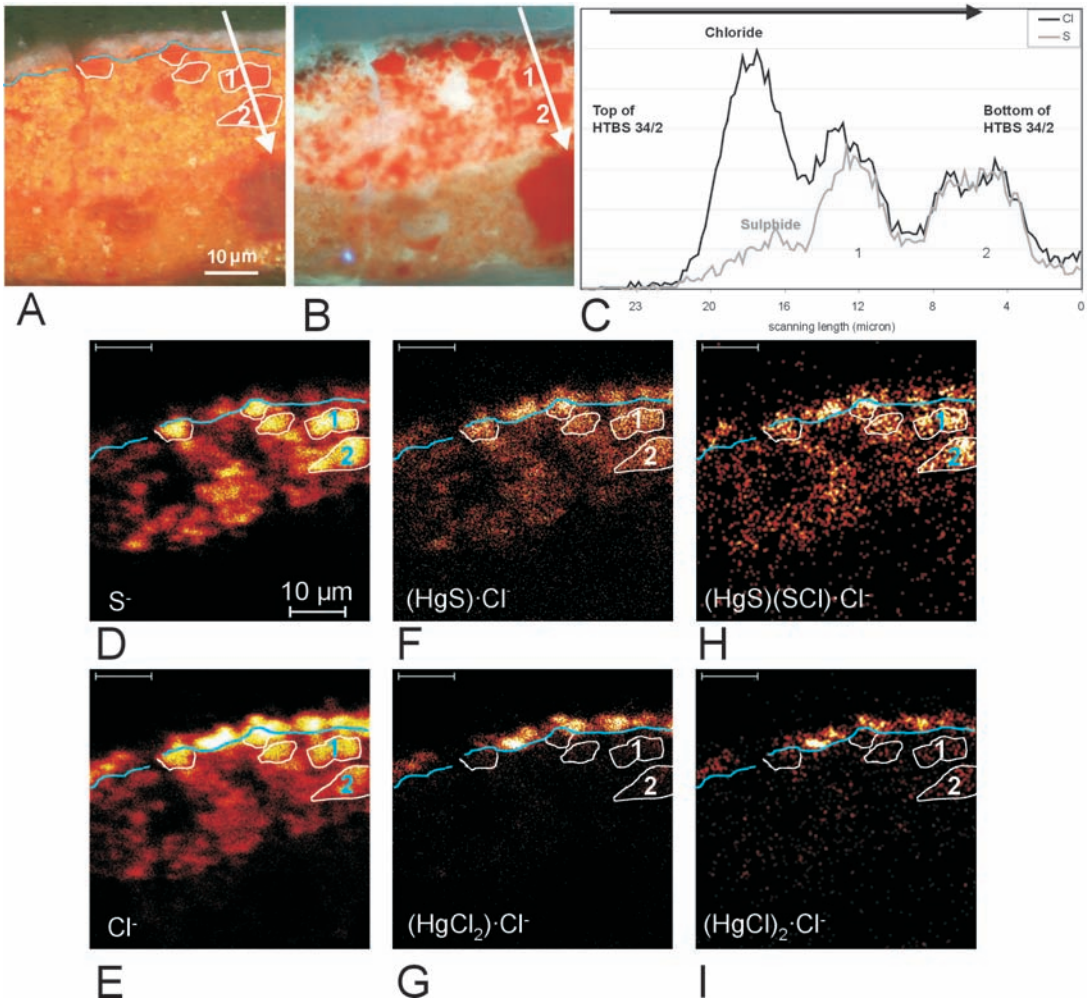

Fig. 4.5 Distribution of sulphur and chloride and the molecular distribution in a partially degraded vermilion paint; the arrow in the light microscopic image (A) and UV-light image (B), which is representing the scanned SIMS area, indicates the direction of the line scan (C). The negative SIMS image of mercury-halogen cluster ions elucidates the position of S^- (D), Cl^- (E), $(HgS)Cl^-$ (F), $(HgCl_2)Cl^-$ (G), $(HgS)(SCl)Cl^-$ (H), $(HgCl)_2Cl^-$ (I) in the partially degraded vermilion paint. The numbers 1-4 in the SIMS images refer to vermilion particles in the corresponding light microscopic images (see coloured version at the end of this thesis).

whereas $(HgS)_n(HgCl_2)\cdot Cl^-$ and $(HgCl)_2\cdot Cl^-$ are only detected in the degraded layer. The SIMS images in Fig. 4.5f-i illustrate this distribution of $(HgS)\cdot Cl^-$, $(HgCl_2)\cdot Cl^-$, $(HgS)(SCl)\cdot Cl^-$ and $(HgCl)_2\cdot Cl^-$ in HSTB 34/2. A contour drawn on the basis of the light microscopic image and the total negative ion image, outlines five red vermilion particles and the boundary in blue between the intact and degraded paint.

Fig. 4.6a-f represent partial negative ion mass spectra of the reference materials HgS, $(HgCl)_2$ and $HgCl_2$ and their mixtures HgS + $(HgCl)_2$ and HgS + $HgCl_2$. The reference materials, $HgCl_2$ and $(HgCl)_2$, are two separate white mercury chloride complexes that are suspected to be present in the degraded vermilion layer of paint cross-section HSTB 34/2. Part of the negative ion mass spectrum of the degraded vermilion paint in paint cross-section HSTB 34/2 is depicted in Fig. 4.6g. The spectrum is acquired after selecting the region of interest (ROI) in the total area analysed (50 μm^2). The SIMS spectrum of the intact vermilion is represented by Fig. 4.6h. Fig. 4.6i represents the calculated isotopic distributions of the ion clusters $(Hg_3S_3)Cl^-$, $(Hg_3S_2Cl_2)Cl^-$, $(Hg_3S_5)Cl^-$, $(Hg_3S_6)Cl^-$. These ions were chosen for calculation because they match the mass window of the relevant cluster ion peak patterns from mercury-halogen cluster ions with 3 mercury atoms in the regions of interest.

The SIMS spectra of the reference materials and their mixtures support the identification of the new products present in the degraded vermilion paint layer of HSTB 34/2. Vertical dotted lines pasted over the mass spectra in Fig. 4.6 divide these into four mass windows corresponding to the four columns in the Table 4.1. Table 4.1 gives an overview of the interpreted mercury-halogen cluster ion patterns in four mass windows deduced from the spectra of the various reference materials and the paint cross-section present (Fig. 4.6 and Table 4.1). In the mass window from 720-750 amu, $(HgS)_3Cl^-$ (*m/z* 726-743) is detected in the mass spectrum of intact and degraded vermilion in HSTB 34/2 (Fig. 4.6g and h). The reference spectra of both mixtures (HgS + $HgCl_2$ and HgS + $(HgCl)_2$) show the same cluster ions (Fig. 4.6e, f), while the spectrum of pure HgS shows a $(HgS)_3S^-$ cluster ion without a chloride ion attached (Fig. 4.6a). In the mass window from 750-790 amu, peaks at 760-781 amu assigned to $(Hg_3S_2Cl_2)Cl^-$ are dominant in the mass spectrum of the degraded vermilion (Fig. 4.6g). The ion cluster $(Hg_3S_2Cl_2)Cl^-$ is only found in the spectrum of the mixture of HgS + $HgCl_2$ (Fig. 4.6f). A relative small amount of $(Hg_3S_4)Cl^-$ and $(Hg_3SCl_3)Cl^-$ in this mass range is detected in the degraded vermilion (these cluster ions partially overlap with the cluster ions of $(Hg_3S_2Cl_2)Cl^-$). In the intact vermilion relatively minor contributions from $(Hg_3S_2Cl_2)Cl^-$ and $(Hg_3S_4)Cl^-$ are detected (Fig. 4.6h). The mass window from 790-820 amu shows $(Hg_3S_5)Cl^-$ and $(Hg_3S_4Cl)Cl^-$ in the mass spectrum of the intact vermilion of HSTB 34/2. The latter cluster ion is found in low yields in the spectrum of the mixture [HgS + $HgCl_2$]. In the

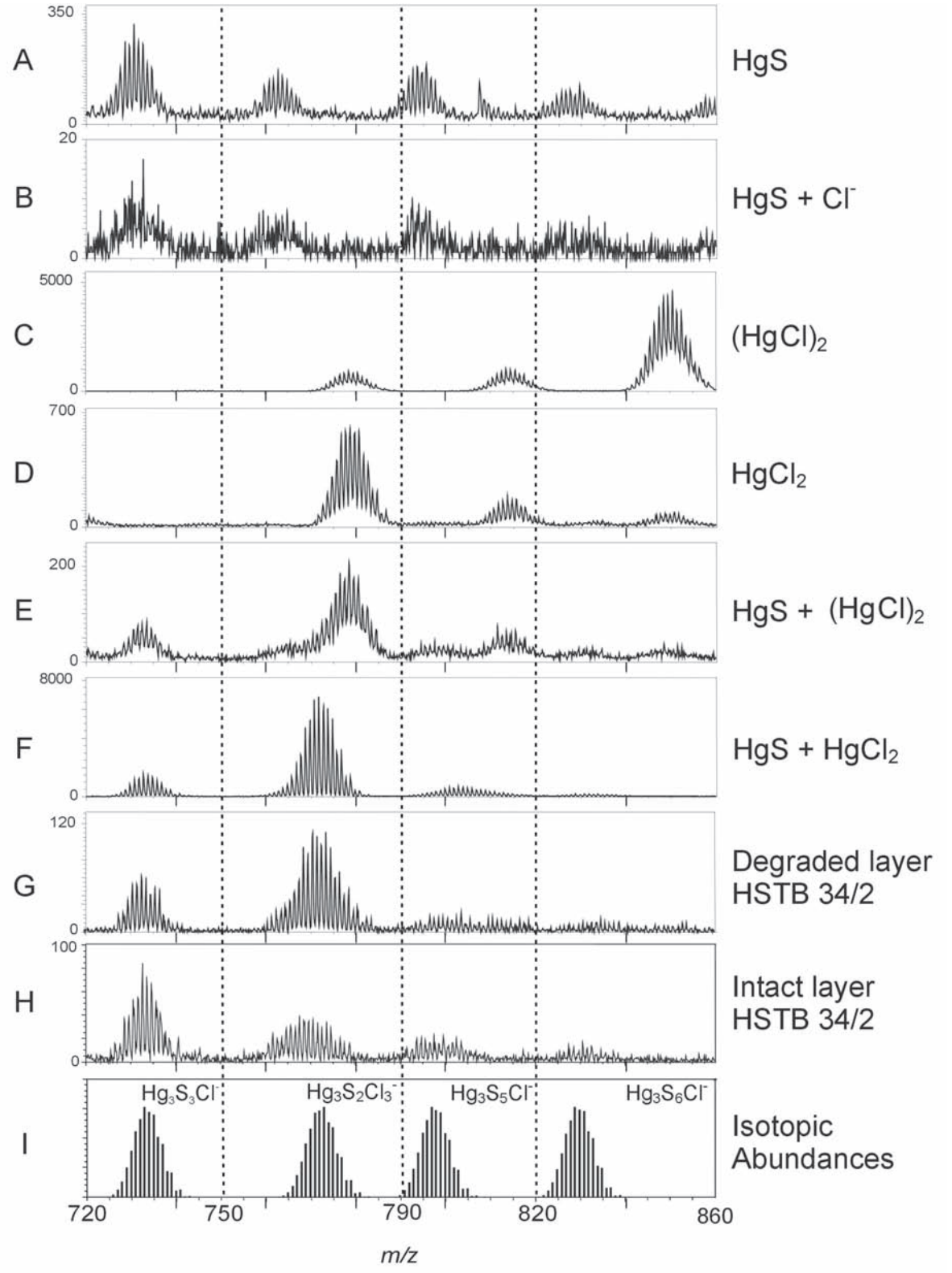

Fig. 4.6 Part of the negative ion mass spectrum in the mass window from 720-860 amu of pure HgS (A), HgS + Cl- ions (B), pure $(HgCl)_2$ (C), pure $HgCl_2$ (D); a mixture of HgS + $(HgCl)_2$ (E); mixture of HgS + $HgCl_2$ (F) and paint cross-section HSTB 34/2 (G). The vertical dotted lines divide the spectra into four mass ranges which correspond with the columns in Table 4.1.

Sample	mass range 720-750 amu	mass range 750-790 amu	mass range 790-820 amu	mass range 820-860 amu
HgS	$(HgS)_3S^-$	$Hg_3S_5^-$	$Hg_3S_6^-$	$Hg_3S_7^-$
HgS + Cl^-	…	…	$Hg_3S_6^-$	-
$HgCl_2$	-	$(Hg_3Cl_4)Cl^-$	$(Hg_3Cl_5)Cl^-$	$(Hg_3Cl_6)Cl^-$
Hg_2Cl_2	$-^-$	$(Hg_3Cl_4)Cl^-$	$(Hg_3Cl_5)Cl^-$	$(Hg_3Cl_6)Cl^-$
HgS + $HgCl_2$	$(HgS)_3Cl^-$	$(Hg_3S_2Cl_2)Cl^-$	$(Hg_3S_2Cl_3)Cl^-$ $(Hg_3S_3Cl_2)Cl^-$ $(Hg_3S_4Cl)Cl^-$	$Hg_3S_6Cl^-$
HgS + Hg_2Cl_2	$(HgS)_3Cl^-$	$(Hg_3Cl_4)Cl^-$	$(Hg_3Cl_5)Cl^-$	$(Hg_3Cl_6)Cl^-$
Degraded layer HSTB 34/2	$(HgS)_3Cl^-$	$(Hg_3S_2Cl_2)Cl^-$ $Hg_3S_4Cl^-$ $Hg_3SCl_3Cl^-$	-	-
Intact layer HSTB 34/2	$(HgS)_3Cl^-$	$(Hg_3S_2Cl_2)Cl^-$ $Hg_3S_4Cl^-$	$Hg_3S_5Cl^-$	$Hg_3S_6Cl^-$

Table 4.1 Overview of the various mercury-halogen cluster ions detected in the negative ion mass spectra in the mass window from of 720-860 amu that originate from spectra of the reference materials, their mixtures and the paint cross-section HSTB 34/2. The four mass ranges correspond to the mass windows indicated in Fig. 4.6.

mass window from 820-860 amu the cluster $(Hg_3S_6)Cl^-$ is detected in low yields in spectra of the paint cross-section as well as in the mixture HgS + $HgCl_2$ (Fig. 4.6f and h and Table 4.1*)*.

Fig. 4.6b represents the SIMS spectrum of the reference material HgS with an excess of chloride ions added as KCl. We conclude that the mercury-halogen cluster ions detected in the paint cross-section are not formed by gas-phase ion chemistry just above the surface after SIMS of HgS and KCl, because $(HgS)_n(HgCl_2)\cdot Cl^-$ and $(HgCl)_2\cdot Cl^-$ are not observed in this spectrum. The exact identification of the composition of the mercury-halogen cluster ions in Fig. 4.6b is difficult as the yields and thus the resolution is low.

4.4 Discussion

The two paint cross-sections investigated that originate from paintings made by two different painters and that were kept under different conditions give similar analytical information on the colour changes in vermilion. The analytical imaging studies on the darkened vermilion oil paint layer in sample MH251/26 demonstrate the degradation phenomena in detail. As light is a requirement for the degradation process, it is concluded that the light must have penetrated the whole affected layer as all particles in sample MH251/26 are homogenously transformed. On the basis of the transition of the red into the black materials observed in the partially degraded particles and the position of the white materials around the black materials, we propose that the black coloured material is formed first. In a later stage the white product is formed from the black reaction product.

Both the SIMS and EDX techniques show relatively high amounts of chloride and relatively low amounts of sulphide in the degraded particles. The relative amount of mercury in the intact and degraded particles is considered to be constant, since the backscattered electron intensity in the BSE image is the same for all phases. The EDX images lead us to conclude that sulphur leaches from the particles in the degraded layer into the environment. However, EDX spot analyses detect sulphur in the organic binding medium of both the degraded and the intact part. The organic binding medium also has been shown to contain aluminium. Sulphur and aluminium are known constituents of the inorganic substrate of red lakes.[10] It is therefore possible that red lake possible has been mixed into the paint although no distinct pigment particles are visible.

The mercury-halogen cluster anions detected in the whole vermilion layer with SIMS are charged by attachment of Cl^- ions. Neutral molecules are known to be anionised by chloride to form a negatively charged complex.[11, 12] The ions $(HgS)_nCl^-$ and $(HgS)_n(SCl)Cl^-$ are found in the intact vermilion paint layer and are representative for intact HgS. $(HgS)_nS^-$, detected in the pure HgS, is not present in the SIMS spectra of the mixtures and may be suppressed by the presence of chloride. Ions from $(HgS)_n(HgCl_2)\cdot Cl^-$ (n = 0-6) are detected and mainly present in the degraded vermilion layer. These types of ions are also formed from the mixture of HgS + $HgCl_2$ but not from the mixture HgS + $(HgCl)_2$. We conclude on the basis of the presence of these types of ions found in the degraded vermilion layer that it is indicative for mercuric chloride ($HgCl_2$). In addition, the ions from $(HgS)_n(HgCl_2)\cdot Cl^-$ detected in SIMS data of a mixture of HgS + $HgCl_2$ indicates that HgS is still present in the degraded vermilion layer, because these ions are absent in the spectra of pure $HgCl_2$. The ions $(HgCl)_2\cdot Cl^-$ are not only representative for $(HgCl)_2$ (calomel), because these ions are also detected in the spectrum of HgS + $HgCl_2$

(part of the spectrum not shown). It is concluded that the presence of calomel in the paint sample cannot be proven with SIMS, because this ion $(HgCl)_2 \cdot Cl^-$ is not characteristic for $(HgCl)_2$ (calomel) and $(Hg_3Cl_4) \cdot Cl^-$ is only detected in the HgS + $(HgCl)_2$ reference mixture and not in the paint sample.

On the basis of our results and literature data, we propose that the transformation of vermilion from red into black materials is a conversion from HgS into Hg(0) and S(0) by a photochemical reaction catalysed by chloride (Step 1 in Fig. 4.7). The conversion of Hg(0) from photo-reduced Hg(II) has been reported both in solid phase[13] and aqueous media.[14, 15, 16, 17, 18, 19] This supports the idea of the light induced conversion of Hg(II)S into Hg(0). After the photo-reduction reaction, the metallic mercury is deposited on the intact HgS surface resulting in a black reaction product. The remaining HgS in the degraded vermilion is identified with SIMS. The metallic mercury is present as nanoparticles, which is supported by the "hot" spots smaller than 100 nm visualised in the BSE-image (Fig. 4.2c and supplementary Fig. 4.1). The Hg(0) precipitation on the vermilion surface has never been proven directly, but has been suggested by other authors.[6, 16, 20] Elementary sulphur is also detected as a product of photo-degraded HgS.[19] The sulphur leaves the paint particles possibly in the form of volatile sulphur oxide, as sulphur has been shown to oxidise to sulphate ions via polythionic acids.[21] Since the sulphur is lost from the particle, it is inferred that a conversion of vermilion to meta-cinnabar is unlikely. The small relative concentration of sulphur still present in the particles is ascribed to intact residual intact vermilion. XRD measurements performed on reconstructions and other paint samples elsewhere by other authors support this conclusion.[1, 2, 4, 7, 9] It is shown that

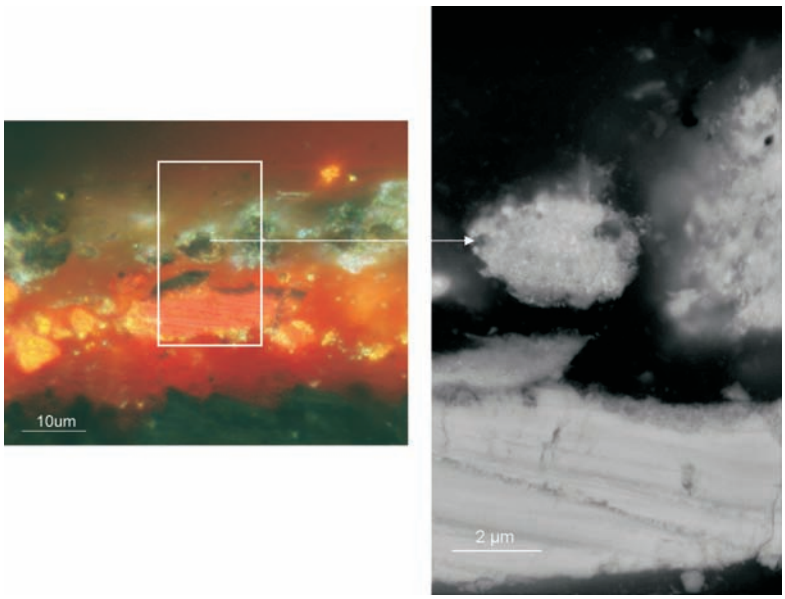

Supplementary Fig. 4.1 The BSE-image visualises a black particle containing hotspots of smaller than 100 nm. These hotspots are nanoparticles of metallic mercury (see coloured version at the end of this thesis).

vermilion is still present in the XRD spectra of the blackened vermilion as is deduced from the decreased intensity of the XRD patterns of vermilion. No black meta-cinnabar was shown in the XRD spectra.

Chlorine plays a dominant role in the light induced blackening phenomenon, as already is suggested in the literature.[7, 9] The much more sensitive surface technique of SIMS demonstrates, in contrast to the EDX results, that chloride is present inside the vermilion particles of both MH 251/26 and HSTB 34/2. The concentration of chloride in the red particles must be below the detection limit of EDX. As small quantities of chloride make vermilion photosensitive[7], the small amounts of chloride detected in the intact vermilion trigger the blackening process. Due to the fact that only small quantities of chloride are necessary to form blackened cinnabar and that other compounds besides chloride ions, such as iodide, enhance the blackening as well, it is concluded that chloride initially acts as a catalyst and is not part of the primary reaction products. The exact minimum concentration of chloride necessary to trigger the process is not known. McCormack states that cinnabar is light stable below 0.01wt% (± 0.01 wt%) chloride, as determined with a wavelength-dispersive microprobe analyser, cinnabar is light stable and that it blackens at a concentration of 0.05 wt% and higher[7].

The exact mechanism of the photo-degradation of vermilion catalysed by chloride is still an open question. We suggest that under the influence of light an electron-hole pair is generated and a photoeletrochemical process takes place, which enables an electron transfer from chlorine anion to mercury and from sulphide back to chloride (i.e. chloride has a catalytic function). Assuming that chlorine anions are oxidised by the positive holes of the valence band of HgS, the valence band edge of HgS must be more positive than the redox potential of Cl^-/Cl_2.[16, 22] The exact position of the valence band edge of HgS is not clear, but the value of this position is expected to be close to the redox potential of Cl^-/Cl_2.[22]

The relatively high quantity of chloride in the degraded part is hard to explain from an original vermilion source alone. We also have to conclude that the chloride is not introduced via the binding medium, as EDX did not detect chloride in the binding medium of the intact area. In order to explain the relatively high yields of chloride ions in the degraded vermilion particles it is necessary to invoke additional source of chlorides. Chloride is possibly transported by diffusion from paint layers positioned lower or introduced from an external source.

After the first transformation, the black product is thought to trap chloride to transform subsequently into a white reaction product. Although the elemental composition (Hg, S, and Cl) of the black and the white phase is the same, the EDX spot analysis shows a higher relative intensity of chlorine and a fairly lower relative intensity of sulphur in the white product (S3) compared to the black product (S1) (Fig. 4.2a and d). SIMS iden-

tifies the mercury chlorine complex $HgCl_2$ in the degraded vermilion layer. Mercuric chloride ($HgCl_2$) has never been identified in paintings before. Calomel $(HgCl)_2$ cannot be identified positively with SIMS, however, Spring *et al.* had identified calomel as the white product in paintings-containing degraded vermilion using Raman microscopy.[9]

The two components in the black product, metallic mercury and residual vermilion, react with chloride supplied by sources external to the vermilion. The residual vermilion reacts with this external chloride to the light sensitive mineral corderoite, which degrades under the influence of light into calomel, metallic mercury and sulphur. Corderoite ($Hg_3S_2Cl_2$) can easily be formed in a mixture of HgS and NaCl solution kept at room temperature after a long period[7, 9] and will after light exposure degrade into a dark grey product containing $(HgCl)_2$.[9] The formation of corderoite could not have taken place in the first degradation steps, because of the high amount of chloride required that is suggested to accumulate after the blackening. The $(HgCl)_2$ formed photo-degrades under normal light into $HgCl_2$ and Hg(0).[23] The metallic mercury, derived from the photo-reduction in the first step, the corderoite and the $(HgCl)_2$, react with chloride to form mercuric chloride $HgCl_2$. In vitro $HgCl_2$ can be formed from metallic mercury via the reaction with chlorine gas or by via the formation of mercury(II)sulphate.[24] The white end product is found around the black product, which means that external sources, light and a higher concentration of chloride are necessary to create the white product.

Fig. 4.7 illustrates the scheme of the proposed mechanisms of the degradation process of the red vermilion into the black and subsequently the white reaction product. The scheme describes the degradation phenomena qualitatively to clarify the process. The products observed in the paint cross-sections are mixed phases and consequently cannot be classified in a single category in the scheme. For example, the black product in sample MH251/26 has a relatively higher concentration of chloride compared to the intact red vermilion. Based on its colour this black product would be classified in the black box after step 1 in the diagram, but a relative increase in chloride is taking place. This accumulation in the black product is indicated in step 2, but a conversion into a white product is not observed with light microscopy. Therefore, the black product would be classified in the box after step 2, which is indicated in the scheme as grey. Furthermore, not all the degraded vermilion is converted into $HgCl_2$ in sample HSTB 34/2, some of the former reaction products are still expected to be present.

The obtained knowledge implies that the quality of the vermilion used in paintings is of significant importance for the changes of preservation of the red colour. Small chloride or other halogen impurities in the vermilion makes the red pigment photosensitive. Chloride present in the medium or derived from other external sources can drive subsequent reactions. Works of art such as easel and mural paintings can be expected to be exposed to light and chlorides.

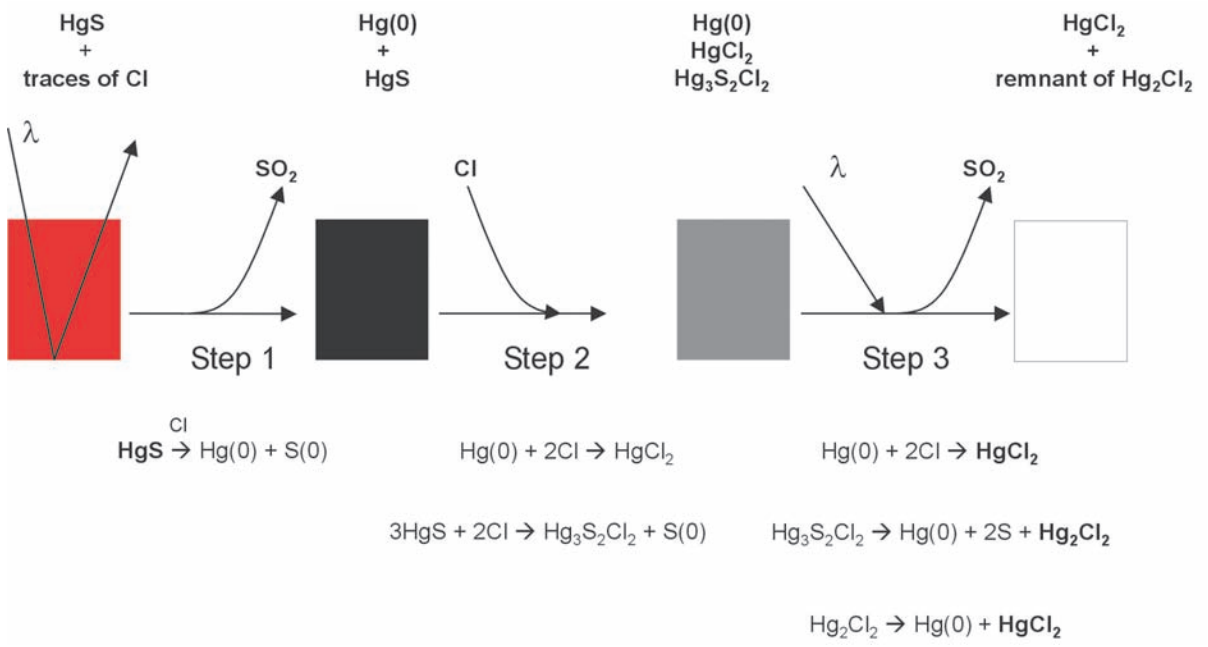

Fig. 4.7 Scheme of the proposed mechanisms of the degradation process of the red vermilion into a black and finally a white product (see coloured version at the end of this thesis).

4.5 Conclusions

Analytical studies on paint cross-sections containing darkened vermilion reveal the light induced degradation phenomena in detail. Light microscopic images reveal two coloured reaction products, a white product positioned above and around a black product. SEM/EDX data give information about the elemental distribution and the structural changes between the three coloured phases. SIMS detects, in contrast to EDX, traces of chloride in the native vermilion The additional benefit of imaging SIMS applied for the first time to investigate this phenomenon in paint cross-sections is that the molecular information from SIMS is able to identify the white reaction product as mercuric chloride. We propose a new hypothesis, which describes a three-step process where black and white reaction products are formed from each other. Chloride acts as catalyst in the first step of the photo-induced chemical degradation of vermilion. In the formed black reaction product, an excess of chloride is accumulated. The black phase will react further with the excess of chloride to form the white product, mercuric chloride. The combination of both techniques, SEM/EDX and SIMS, is essential to elucidate the familiar phenomenon of 'blackening of vermilion' in detail.

4.6 Acknowledgements

We are grateful to Linnaea Saunders, Kress Fellow 2003 - 2004, Mauritshuis, The Hague, The Netherlands who provided us the paint cross-section MH251/26. We would also like to thank Lidwien Speleers, AMOLF, Amsterdam, The Netherlands for providing the paint cross-section HSTB 34/2.

4.7 References

1 R. Grout, A. Burnstock, *A study of the blackening of vermilion*, Zeitschrift für Kunsttechnologie und Konservierung 2000, Hft 1, p. 15-22.

2 R.L. Feller, *Studies on the darkening of vermilion by light*, National Gallery of Art, Report and Studies in the History of Art 1967, Washington, DC, 1967.

3 R.J. Gettens, R.L. Feller, W.T. Chase, *Madder and alizarin*, In: Artists' pigments, vol. 2, A. Roy (Ed.), Oxford University Press, New York, 1993, p. 167-168.

4 V. Daniels, *The blackening of vermilion by light*, In: Recent Advances in the Conservation and Analysis of Artifacts, J. Black (Ed.), Summer School press, London, 1987, p. 280-282.

5 R.S. Davidson, C.J. Willsher, *The light-induced blackening of red mercury(II)sulphide,* Journal of the Chemical Society Dalton Transactions, 3, 1981, p. 833-835.

6 R.M. Dreyer, *Darkening of cinnabar in sunlight*, American Mineralogist, 23, 1938, p. 457-460.

7 J.K. McCormack, *The darkening of cinnabar in sunlight,* Mineralium Deposita, 35, 2000, p. 796-798.

8 R.S. Davidson, C.J. Willsher, C.L. Morrison, *Influence of some solvents and solutes on illuminated red mercury(II)sulphide electrodes*, Journal of the Chemical Society Faraday Transactions 1, 78, 1982, p. 1011-1019.

9. M. Spring, R. Grout, *The blackening of vermilion: an analytical study of the process in paintings,* National Gallery Technical Bulletin, 23, 2002, p. 50-61.

10 H. Schweppe, J. Winter, *Vermilion and cinnabar*, In: Artists' pigments*,* vol. 3, E. West FitzHugh (Ed.), Oxford University Press, New York, 1997, chapter 4.

11 G.S. Groenewold, *et al., Characterization of copper chloride cluster ions formed in secondary ion mass spectrometry*, International Journal of Mass Spectrometry, 178, 1998, p. 19-29.

12 A. Delcorte, *Fundamental aspects of organic SIMS,* In: ToF-SIMS: Surface Analysis by Mass Spectrometry, J.C. Vickerman, D. Briggs (Eds.), IM Publication and Surface Spectra Limited, 2001, p. 183.

13 M.S. Gustin, H. Biester, C.S. Kim, *Investigation of the light-enhanced emission of mercury from naturally enriched substrates*, Atmospheric Environment, 36, 2002, p. 3241-3254.

14 Y.H. Hsieh, S. Tokunaga, C.P. Huang, *Some chemical reactions at the HgS(s)-water interface as affected by photoirradiation,* Colloids and Surfaces, 53, 1991, p. 257-274.

15 M. Ravichandran, *Interactions between mercury and dissolved organic matter- a review*, Chemosphere, 55, 2004, p. 319-331.

16 B. Pal, S. Ikeda, B. Ohtani, *Photoinduced chemical reactions on natural single crystals and synthesized crystallites of mercury (II) sulfide in aqueous solution containing naturally occur ring amino acids*, Inorganic Chemistry, 42, 2003, p. 1518-1524.

17 M.I. Litter, *Heterogeneous photocatalysis transition metal ions in photocatalytic systems*, Applied Catalysis B-Environmental, 23, 1999, p. 89-114.

18 D. Strömberg, A. Strömberg, U. Wahlgren, *Relativistic quantum calculations on some mercury sulfide molecules*, Water Air and Soil Pollution, 56, 1991, p. 681-695.
19 S. Okouchi, S. Sasaki, *Photochemical behaviour of mercury ore in water*, Environment International, 9, 1983, p. 103-106.
20 M.S. Gaustin, R.A. Maxy, P. Rasmussen, *Mechanisms influencing the volatile loss of mercury from soil*, In: Symposium volme of Air Pollutance, Cary, NC, September 1998.
21 K. Naito, S. Takei, T. Okabe, T., *The chemical behavior of low valence sulfur compounds. II. Thin-layer chromatographic separation and photometric determination of low valence sulfur compounds*, Bulletin of the Chemical Society of Japan, 43, 1970, p. 1360-1364.
22 Personal communication with professor B. Ohtani (Catalysis Research Center, Hokkaido University, Japan), 2004.
23 C. Chambers, A.K. Holliday, In: Modern Inorganic Chemistry, Butterworth & Co, London, 1975, p. 437.
24 A.F. Holleman, E. Wilberg, In: Inorganic Chemistry, Academic Press, San Diego, 2001, p. 1310.